Virtual Shaping on NACA 0015 by Means of a High Momentum Coefficient Synthetic Jet

Matteo Orazi[1], Davide Lasagna[2] and Gaetano Iuso[3]
Politecnico di Torino, Turin, 10129, Italy

[Received date; Accepted date]

ABSTRACT

Results concerning flow control on a NACA 0015 airfoil using high power synthetic jets are presented for low incidences and for Reynolds numbers ranging from 132000 to 425000. The forcing was operated through a spanwise slit positioned near the leading edge at x/c = 1.25% or at x/c = 10% on the upper surface. Static pressure distribution measurements around the airfoil, wake surveys and smoke flow visualizations were performed. Pressure distributions were significantly modified around the injection location, showing an area of intense suction which increased the lift and strongly affected the drag. Flow visualizations highlighted that the intense suction was due to a virtual shaping effect caused by the formation of a recirculation bubble capable of displacing the streamlines. Low momentum deficits in the wake velocity distributions and, in certain conditions, jet-like flow were observed for the forced cases. Finally, a scaling law relating the bubble size to the forcing intensity is proposed.

1. INTRODUCTION

Since their introduction as a flow control device in the 90s by Glezer and his coworkers, synthetic jets have received increasing attention. In recent years many applications of these flow control devices have been proposed and applied to a large variety of flows. Smith and Glezer [1] showed the mechanisms of formation and evolution of a synthetic jet in still air condition while a complete review concerning the fundamentals of synthetic jets and their flow control applications was presented by Glezer and Amitay [2]. Cater and Soria [3] performed an experimental comparison between synthetic and continuous jets using Particle Image Velocimetry and dye flow visualizations. The authors show that the larger spreading rate and decay, which characterize the synthetic jet, are due to the structural differences in the near field. Rizzetta *et al.* [4] performed direct numerical simulation of both the flow within the actuator cavity and the jet flow surrounding the orifice, using the unsteady compressible Navier-Stokes equations. Simulations showed the formation and evolution of the inner and outer flow investigating the effects of several parameters such as the cavity height and the Reynolds number. Compared to the traditional steady actuation, based on continuous blowing or suction, oscillatory actuation operated by means of a synthetic jet may lead to better results for separation control applications as shown by Seifert *et al.* [5] for different airfoils at Reynolds numbers up to $1.2 \cdot 10^6$. Furthermore synthetic jets show interesting properties for cooling applications due to the higher turbulence level as shown by Trávníček and Tesař [6].

Important control parameters for synthetic jets are the momentum coefficient C_μ and the non-dimensional frequency F^+. With respect to the non-dimensional actuation frequency F^+, two different approaches of flow control can be carried out. One use is characterized by forcing frequency $F^+ \approx O(1)$ which corresponds approximately to the non-dimensional frequency shedding in the wake. Glezer *et al.* [7, 8] reported that the actuation couples to and drives the shedding, modifying the circulation over the entire airfoil and producing a Coanda-like deflection of separated shear layer of the stalled airfoil. The second approach is called "Virtual Aero-shaping" and is characterized by $F^+ \approx O(10)$. In the study of

[1] PhD Student, Aerospace Department, Politecnico di Torino, matteo.orazi@polito.it.

[2] PhD Student, Aerospace Department, Politecnico di Torino, davide.lasagna@polito.it.

[3] Professor, Aerospace Department, Politecnico di Torino, gaetano.iuso@polito.it, http://www.flowcontrolgroup.polito.it

Smith *et al*. [9] the virtual shaping actuation is located upstream from the separation point and forms a controlled interaction domain with the cross flow near the injection orifice. As shown in the works of Honohan *et al*. [10, 11], the interaction region between a high-frequency synthetic jet and the external flow over a 2-D cylinder displaces the streamlines of the external flow, inducing a "virtual" change in the shape of the surface.

Numerous experimental and numerical investigations demonstrate the effectiveness of synthetic jets for flow control over airfoils. The numerical study proposed by Rehaman and Kontis [12], employing a synthetic jet located on the upper surface at 28% of chord length on a NACA 0015 at a Reynolds number of 360000, showed an augmentation of the lift coefficient up to 14% for an angle of attack $\alpha = 15°$ and a forcing frequency $F^+ = 18.67$. The results of the numerical investigation suggest that lift is increased when the synthetic jet is located far away from the separation point, on the upstream side, while drag reduction is achieved when the slot is located close to the separation point. The experimental study carried out by Gilarranz and Rediniotis. [13], showed the effects of a high power tangential synthetic jet located at 12% of chord length on NACA 0015 airfoil. The tests were conducted at $Re = 896000$, for angles of attack between $-2° < \alpha < 29°$ and for a momentum coefficient C_μ in the range from 0.003 to 0.012. At small angles of attack, from 0° to 10°, increasing the actuation frequency caused an increase of the lift curve slope up to 5%, varying linearly with the frequency. The stall in no-forcing conditions occurred at $\alpha = 12°$ while the use of the synthetic jet delayed it to $\alpha = 18°$, increasing the maximum lift coefficient up to 80%. Moreover, there was no significant change in drag for $\alpha < 10°$, while for $10° < \alpha < 18°$ the drag coefficient exhibited a reduction with respect to the baseline case that was due to the suppression of the separated region over the airfoil. You and Moin [14] obtained a good agreement with the previous results through Large Eddy Simulation. Duvigneau and Visonneau [15] also compared their results using URANS code with those obtained experimentally by Gilarranz and Rediniotis [13]. The jet was inclined by $\gamma = 35°$ and the forcing frequency was equal to $F^+ = 0.25$, in comparison with the $\gamma = 10°$ and $F^+ = 1.29$ pertaining to the experimental investigation of Gilarranz and Rediniotis [13]. Using an automatic optimization algorithm, the results showed that the stall was postponed to $\alpha = 22°$ and the maximum lift coefficient was increased by about 32%.

Mittal and Rampunggoon [16] performed numerical simulations investigating the possibility of generating large recirculation bubbles in a flow on a flat plate, using synthetic jets. The authors confirmed the presence of such bubbles originating from the interaction and more importantly established the conditions required for their formation. A simple scaling law linking the size of the mean recirculation bubble to the characteristics of the external flow and of the forcing was proposed in order to give indications of the operational synthetic jet regime which creates virtual shaping.

The contribution of the present work touches several aspects. High power actuators, which allowed the investigation of the virtual shaping mechanism over a wide range of the forcing parameters, were developed. The momentum coefficients employed were, in fact, one to two orders of magnitude above most of the studies present in literature reaching the limits of the virtual shaping for which the separation of flow occurs. In addition to pressure distributions, the virtual shaping phenomenon was clearly evidenced through flow visualizations. In particular, the formation of recirculation bubbles due to virtual shaping were mainly observed in numerical experiments while only few experimental results are available in literature. The presence of a "thrusting effect" introduced by intense virtual shaping in the neighborhood of the leading edge was observed and an analogy with the flow field of "flapping airfoils" was found and discussed. Furthermore the effect of the injection location on the virtual shaping mechanisms was investigated. Finally, a simple scaling law, linking the size of the bubble to the momentum coefficient based on the momentum thickness of the boundary layer approaching the injection slit, is presented.

2. EXPERIMENTAL SETUP AND DATA REDUCTION

The wind tunnel used was a blowing open-return type with closed test section with a turbulence level of about 0.4%. The contraction area ratio was equal to 28.6 allowing a maximum velocity of $V_\infty = 22$ m/s. The test section was characterized by height, width and length equal to 0.9m, 0.4m and 1m respectively. A preliminary investigation was performed to verify the flow quality in three different cross sections of the test section. The total pressure maximum deviation from the value measured at the centre of each cross section was equal to 1.2%.

The model wing was characterized by a NACA 0015 airfoil and was mounted between the two vertical walls of the test section. The chord length was equal to $c = 0.4$ m and the span to chord ratio is

equal to $b/c = 1$. The forcing was operated through two rectangular independent slits extending along the spanwise direction and positionable at $(x_{slit}/c)_1 = 1.25\%$ and $(x_{slit}/c)_2 = 10\%$ from the leading edge by using exchangeable cover plates as shown in Fig. 1. The slits were realized to achieve a normal injection with respect to the surface of the airfoil. In order to avoid a geometric modification of the airfoil and especially to facilitate the formation of the synthetic jet [17], the slits were characterized by sharp edges. Under each slit a plenum chamber was positioned inside the wing, covering the whole span and extending up to $x/c = 0.15$ in the streamwise direction. This configuration was necessary to obtain a good spanwise homogeneity of the synthetic jet. A preliminary study on the uniformity of the synthetic jet showed, in fact, that a single slit configuration generates a synthetic jet which is stronger on the opposite side with respect to the actuator connection.

Connecting the actuators on both sides of the model improves the 2D characteristics of the synthetic jet but an acceptable flatness of the spanwise velocity distribution in the central part of the slit was not achieved. This goal was instead obtained dividing the global plenum chamber into two distinct symmetrical plenum chambers. The slit width h was equal to 1 mm ($h/c = 0.25\%$) and covered a spanwise length equal to 196 mm on each part of the wing (± 49% of the span). An inclinometer for the measurement of the pitch and the roll angles was mounted inside the wing profile in the center of the model to measure the angle of attack and to ensure a zero roll angle at all times. The wing model was equipped with 124 static pressure taps distributed along two streamwise sections on the upper and lower surface at $z/B = \pm 18.75\%$. Along the spanwise direction, at different distances from the leading edge, four ($(x/c)_{up} = 0.25\%$, 3.75%, 19.75%, 38.75%) and two ($(x/c)_{low} = 19.75\%$, 38.75%) rows of pressure taps were installed on the upper and lower surface respectively.

Figure 1 shows the location of the pressure taps and the synthetic jet slit. The connection points between the plenum chambers and the actuators are also indicated.Two mechanical crank-rod piston systems taken from airplane model engines were used to construct a single actuator. On each side of the wing model one actuator was mounted operating in-phase and in boxer configuration. In this way vibrations were greatly reduced avoiding perturbations on the wing profile. In figure 2 the scheme of such actuators is reported.

Each engine was characterized by a displacement equal to 20cc (bore 30.4 mm; stroke 27.5 mm). On the top of each cylinder a Plexiglas cylinder-head with a steel elbow was mounted. A rubber tube

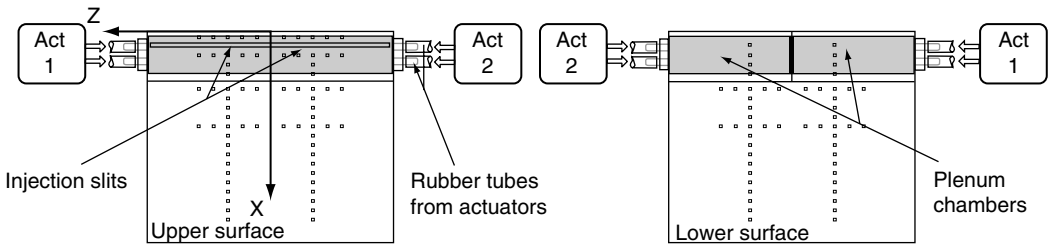

Figure 1. Wing model reporting the location of synthetic jet actuators, slits and pressure taps.

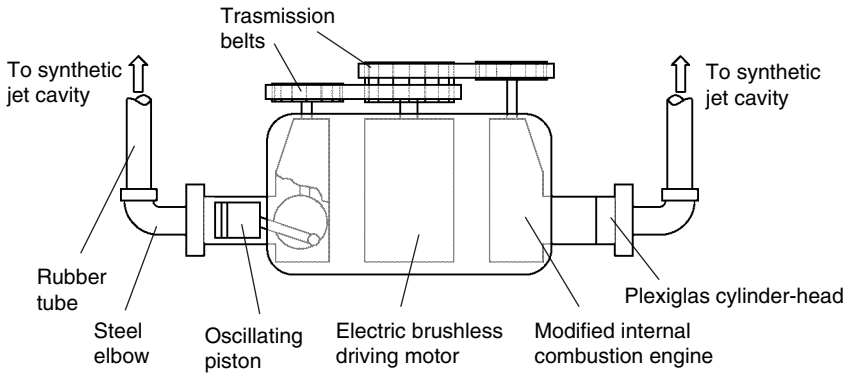

Figure 2. Synthetic jet actuator scheme.

provided feeding to the synthetic jet cavity through a direct connection between the steel elbow and the cavity itself. A brushless electrical motor provided motion to the mechanical crank-rod systems by means of transmission belts and gear wheels. The forcing frequency f was varied through control of the angular speed of the brushless motor.

The non-dimensional frequency defining the appropriate oscillating forcing characteristics was defined as:

$$F^+ = \frac{fc}{V_\infty} \tag{1}$$

where c and V_∞ are the chord of the wing airfoil and the undisturbed upstream velocity respectively. Physically F^+ represents the ratio between the flying time of a particle to cover the chord length and the period of oscillation of the synthetic jet.

A miniature total pressure probe with an external diameter equal to 0.25 mm was used to measure the synthetic jet velocity distributions in different cross sections in still air conditions in order to characterize the synthetic jet strength. The total pressure probe was moved across the slit width using a motorized translation stage with a maximum displacement equal to 150 mm, an accuracy of 0.01% of the full scale and a selectable speed in the range 0.15 - 8 mm/s. In order to avoid regions of reversed flow during the characterization of the synthetic jet, measurements were performed at a distance from the exit section equal to 5 times the slit width. Along the spanwise direction, measurements were performed in three sections for the left slit and in six sections for the right slit. For each transversal position six velocity profiles were acquired and averaged to obtain the mean velocity profile. The maximum value for each mean velocity profile was taken to define the spanwise velocity distribution of the synthetic jet. The average value of the spanwise velocity distribution V_j was evaluated (excluding the values near the end of the slit) and used to calculate the momentum coefficient of the synthetic jet using the following expression:

$$C_\mu = \frac{hV_j^2}{cV_\infty^2} \tag{2}$$

For the type of actuator employed C_μ and F^+ are linked. However it was chosen for its capability to generate very high momentum coefficient synthetic jets with a compact and relatively simple configuration. The same choice was made by Gilarranz and Rediniotis [13], for a separation control application.

Wake surveys were carried out downstream of the model at a distance from the trailing edge equal to $x/c = 0.5$. The probe used was a total pressure rake consisting of 31 steel tubes with an inner diameter of 1mm. The spacing of the total pressure probes was 5 mm with the exception of the first and the last three probes, spaced at intervals of 10 mm. The rake was 170 mm long.

Static and total pressures were sampled through two digital differential 16 channels multi-manometers Scanivalve Corp, model DSA 3217. The full scale range was ±10in H_2O and the accuracy was 0.2% of the full scale. Pressure data was collected via Ethernet using TCP/IP protocol. The DSA 3217 incorporates temperature compensated piezoresistive pressure sensors characterized by 16bit A/D converter resolution. Static pressure distributions around the model were sampled for 3 minutes at a rate of 20 Hz in order to provide a sufficient convergence of the mean value. Due to the higher level of unsteadiness, wake analysis was performed by sampling over 5 minutes with the same sampling rate. Smoke flow visualizations were also carried out by means of a commercial smoke generator injecting upstream of the leading edge of the model which was then highlighted using a light-sheet.

Lift coefficient was computed by integrating the static pressure distribution over the model while wake surveys allowed estimation of the drag coefficient through the momentum balance applied to a control region around the wing.

3. RESULTS

The first results presented concern the characterization of the isolated synthetic jet. Next, pressure distributions and wake velocity profiles for the forced cases are shown in comparison with the results

of the baseline flow. The most significant smoke flow visualizations are then shown. Incidences were investigated ranging from $\alpha = 0.5°$ to $\alpha = 9°$, for three chord based Reynolds numbers; $Re_1 = 132000$, $Re_2 = 265000$ and $Re_3 = 425000$. Higher angles of attack were not tested due to the increasing effects introduced by the corner flow. Finally some considerations on the key mechanisms of the virtual shaping and their effects on the aerodynamic characteristics of the airfoil are presented together with a simple scaling law.

3.1. Synthetic Jet Characterization

Table 1 reports the values of the mean synthetic jet velocity V_j obtained for frequencies ranging from 40 to 80 Hz and the resulting momentum coefficient C_μ and non-dimensional forcing frequency F^+ that would have been obtained assuming the same V_j for chord based Reynolds numbers equal to 132000, 265000 and 425000.

For each Reynolds number, as F^+ increases the corresponding momentum coefficient also rises. As can be seen, with the present actuators it is possible to experience high values of the forcing parameters and especially for the momentum coefficient, if compared with most of the values of C_μ present in literature.

Table 1. Synthetic jet Characterization

F	V_j	$Re = 132000$		$Re = 265000$		$Re = 425000$	
Hz	*m/s*	F^+	C_μ	F^+	C_μ	F^+	C_μ
40	26.73	3.2	0.078	1.6	0.020	1	0.008
60	31.60	4.8	0.109	2.4	0.027	1.5	0.011
70	34.90	5.6	0.133	2.8	0.033	1.75	0.013
80	38.28	6.4	0.160	3.2	0.040	2	0.016

3.2. Pressure Distributions

The chordwise distributions of the pressure coefficient obtained in the case of natural flow and different forcing conditions for $\alpha = 3°$ and $Re = 265000$ are reported in Fig. 3 in the case of $(x/c)_{slit} = 1.25\%$.

The results reveal that forcing significantly modifies the pressure distribution in the neighborhood of the injection slit. This modified region enlarges as the forcing frequency increases and extends approximately from the injection slit location up to $x/c = 0.35$ for $F^+ = 3.2$. Very intense suction peaks are present and a value of $Cp = -3.14$ can be observed for the maximum forcing condition. A more extended pressure recovery region is present downstream of the suction peak with respect to the unforced flow, also highlighting a slower pressure recovery downstream of the suction regions resulting in a reduced adverse pressure gradient. On the other hand the lower surface is completely unaffected by the forcing. Furthermore as a consequence of the actuation, the center of pressure was moved toward the leading edge from $x/c = 28.6\%$ of the baseline case to $x/c = 22.7\%$ for $F^+ = 3.2$.

The data shown in Fig. 3 closely resembles the pressure distribution obtained by Tuncer and Platzer [18] on a flapping airfoil as it passes the mean position downwards. In fact they observe an intense suction peak around the leading edge which was sufficiently high to generate thrust.

The pressure drag coefficient was evaluated by integrating the distributions of Fig. 3, and was found to be positive only in the case of natural flow. The drag coefficient decreased when forcing was increased, reaching a minimum of $C_{dp} = -0.029$ for $F^+ = 3.2$. Although this coefficient does not take friction drag into account and is also susceptible to errors due to the small integration step along the y axis, nevertheless it gives an indication of the effect of forcing on pressure drag. Detailed analysis of the drag coefficient will be discussed in the next section.

Chordwise distributions of the pressure coefficient for $\alpha = 3°$, at Reynolds number 425000, are shown in Fig. 4.

Pressure distributions here are similar to those of the previous case. However forcing effectiveness decreases because, at the same dimensional forcing frequency, a higher Reynolds number also results in lower values of the non-dimensional forcing frequency. Close to the leading edge the pressure coefficient changes from $C_p = -1.05$ in the case of natural flow to $C_p = -2.1$ for $F^+ = 2$. Furthermore as

can be observed, at a higher Reynolds number for the lowest forcing intensity only a weak suction peak occurs. Also for this Reynolds number the lower surface is unaffected by forcing.

The streamwise pressure distributions achieved for $\alpha = 3°$ for the lowest Reynolds number are shown in Fig. 5.

In this forcing condition the pressure distribution is greatly affected on account of the high value of the reduced forcing parameters. The pressure coefficient reaches a very high peak of about $C_p = -5.7$ compared to the natural flow case with a minimum pressure coefficient of −1.1.

The pressure distributions for a Reynolds number of 132000 and $\alpha = 6°$ are shown in Fig. 6.

The highest forcing effects on the pressure distributions were found for this incidence and Reynolds number. In fact the modifications are significant on both sides of the airfoil although the upper surface is still the most affected. The suction peak increases with the non-dimensional forcing frequency, reaching the minimum value of $C_p = -9.2$ when at $x/c = 3.75\%$ for $F^+ = 4.8$.

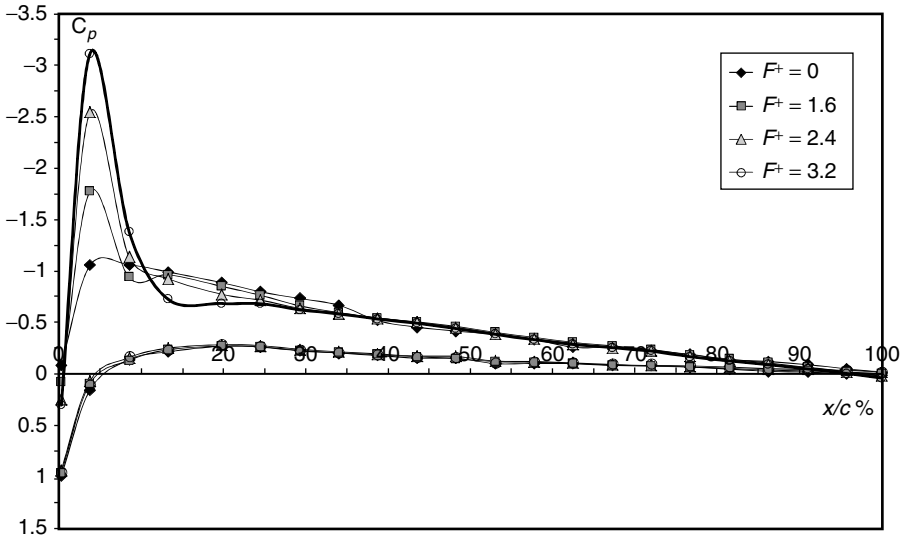

Figure 3. Streamwise pressure coefficient distributions for $\alpha = 3°$, $Re = 265000$, $(x/c)_{slit} = 1.25\%$.

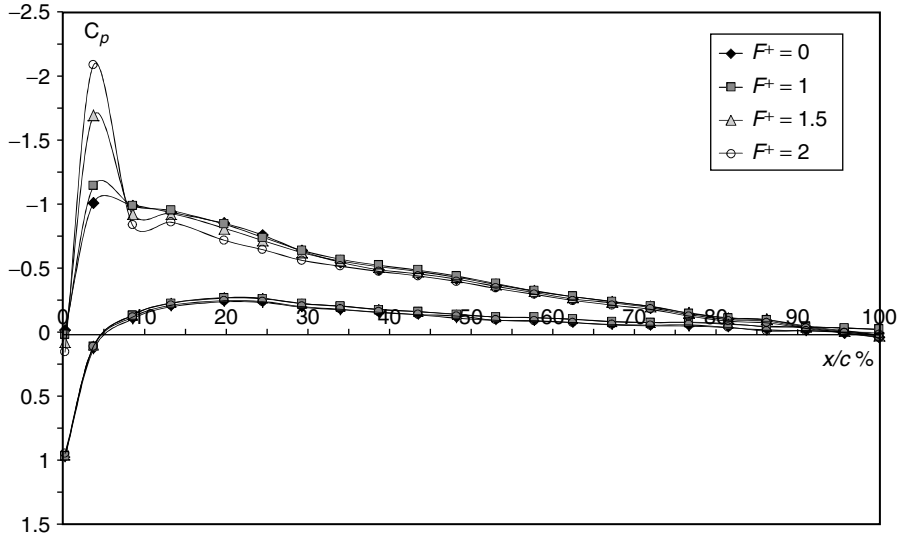

Figure 4. Streamwise pressure coefficient distributions for $\alpha = 3°$, $Re = 425000$, $(x/c)_{slit} = 1.25\%$.

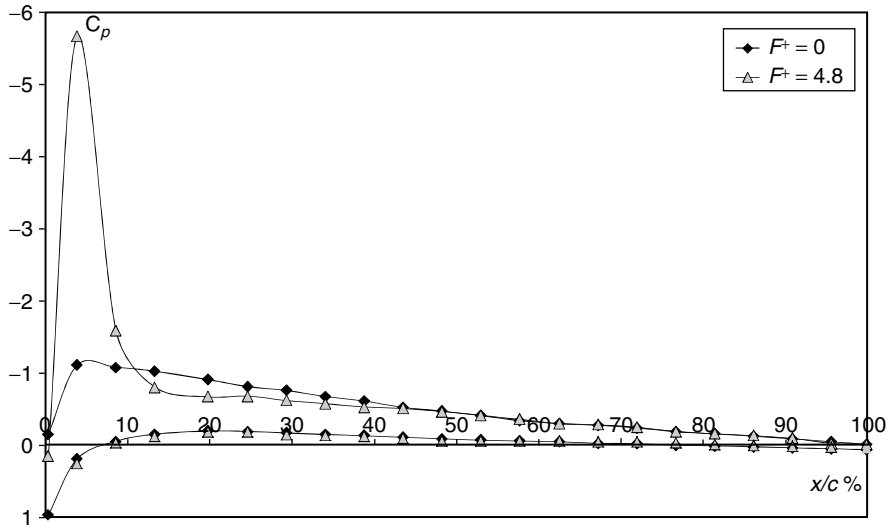

Figure 5. Streamwise pressure coefficient distributions for $\alpha = 3°$, $Re = 132000$, $(x/c)_{slit} = 1.25\%$.

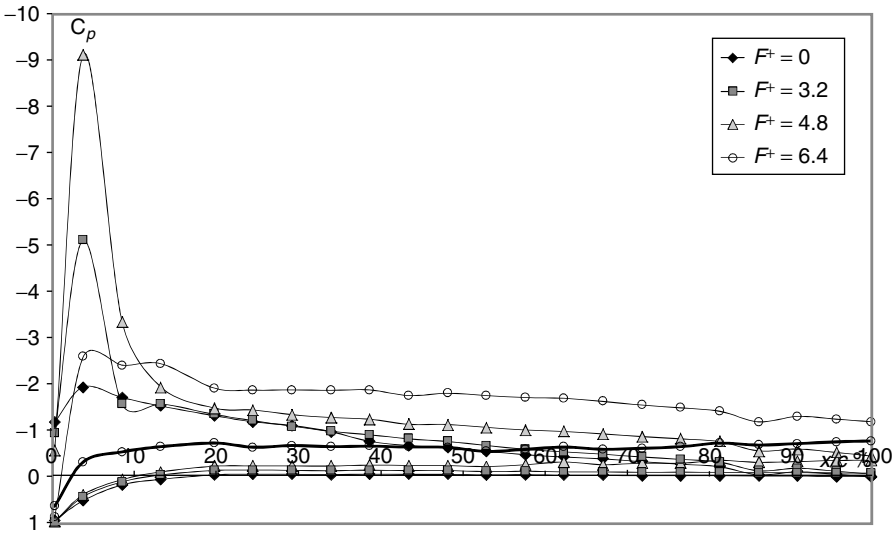

Figure 6. Streamwise pressure coefficient distributions for $\alpha = 6°$, $Re = 132000$, $(x/c)_{slit} = 1.25\%$.

As shown in Fig. 6 for $F^+ = 6.4$ the flow separation occurs close to the leading edge as can be seen from the nearly constant pressure distribution on the upper surface of the wing. At a low Reynolds number the momentum of the synthetic jet is intense enough to determine flow separation close to the injection point without any reattachment. As will be shown in the next section, such forcing conditions cause a notable increase of drag while maintaining almost the same level of lift. This behavior is strictly related to the breakdown of the recirculation bubble as will be documented in the flow visualization section. From this point of view, at very intense forcing, the separated flow gives rise to "virtual aero-braking" application. This effect is interesting for a practical application because it is obtained without the extension of solid surfaces from the wing.

In the following figures 7a, 7b, and 7c the pressure distributions for $\alpha = 0.5°$, $\alpha = 6°$ and $\alpha = 9°$ respectively are presented for $Re = 265000$ and for different forcing frequencies.

As can be observed at all three angles of attack the suction regions are present near the injection slit around the leading edge as in the previous cases. Moreover the value of the peaks increases together with

F^+ and the pressure distributions are influenced only on the upper surface up to about x/c = 25%, as in the case of α = 3°. For α = 0.5° it appears that low values of forcing (F^+ = 1.6) does not substantially affect the pressure distribution. This result is in good agreement with the results reported by many authors such as Rehaman and Kontis [12], Ciuryla *et al.* [19], and Cui *et al.* [20] who seem to find only negligible effects of the synthetic jets on the external flow when using low values of the forcing parameters at low incidence angles. For higher incidence (α = 6° in Fig. 7b and α = 9° in Fig. 7c) the pressure distributions show modifications also at the lowest forcing frequency. Nevertheless more intense suction regions around the injection slot are observed for α = 6° with respect to the incidence α = 9°.

To evaluate the effect of a change in injection location, the slit was placed further downstream, at x/c = 10%. Figure 8 reports the results obtained for α = 3° and Re = 265000 for baseline flow and forced flow for F^+ = 3.2. The result obtained in the same conditions for the slit placed at x/c = 1.25% is also reported for comparison.

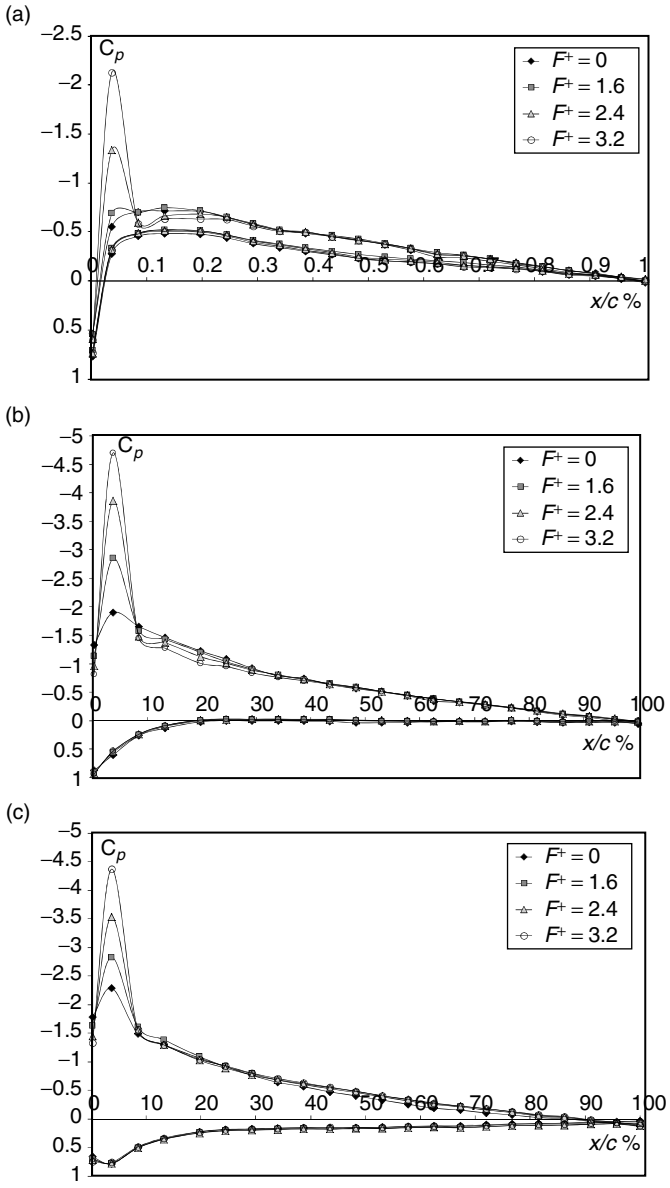

Figure 7. Streamwise pressure coefficient distributions for Re = 265000, $(x/c)_{slit}$ = 1.25%: (a) α = 0.5°; (b) α = 6°; (c) α = 9°.

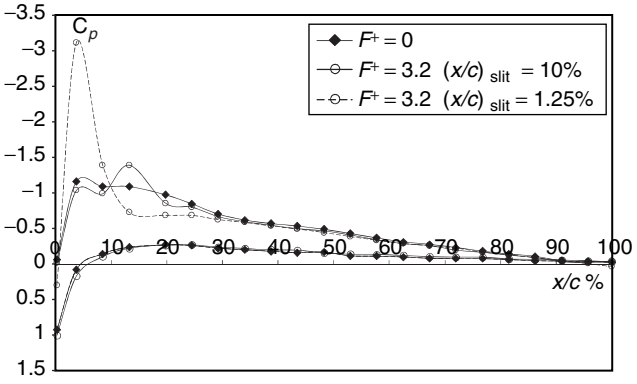

Figure 8. Streamwise pressure coefficient distributions for $\alpha = 3°$, $Re = 265000$, $(x/c)_{slit} = 10\%$.

The pressure distributions in the forced case is much less affected when the slit is located at $(x/c)_{slit} = 10\%$ although a very weak suction peak still forms in proximity to the slit. Results at different incidences, not reported here, showed that, for this position of the slit, an increase of the angle of attack leads to a reduction of the suction region. For $\alpha > 6°$ the pressure distributions do not show significant differences with respect to the baseline case.

From the previous results it appears that the best interaction giving rise to intense suction regions takes place when the injection slit is placed in the region of maximum velocity, very close to the leading edge. Several authors have confirmed a greater efficacy of forcing when the injection was positioned closer to the leading edge. In particular Akçayöz et Tuncer [21] conducted a numerical study on a NACA 0015 showing that higher lift-to-drag ratios are obtained for the injection point moving towards the leading edge and for the highest available value of the momentum coefficient.

The presence of intense suction around the region of interaction suggests that the streamlines are deflected from their natural evolution causing higher local velocity of the external flow due to the presence of a bubble of recirculation flow, as documented also by Gordon and Soria [22], by Mittal and Rampunggoon [16] and as will be shown by flow visualizations. The flow behavior around the injection area is very similar to that generated by a local surface modification. A simple comparison between the experimental results and the Xfoil numerical code was done with the aim of showing the analogy between a virtual and a real local modification of the geometry. The shape of the airfoil was modified adding a bump downstream of the position of the synthetic jets slit. The transition was forced at $x/c = 1.25\%$, where the injection point is located.

Results for $\alpha = 3°$ are shown in Fig. 9 which also reports the geometric shape used during the numerical simulation. The solid shape was evaluated by trial and error to reproduce at best the experimental results.

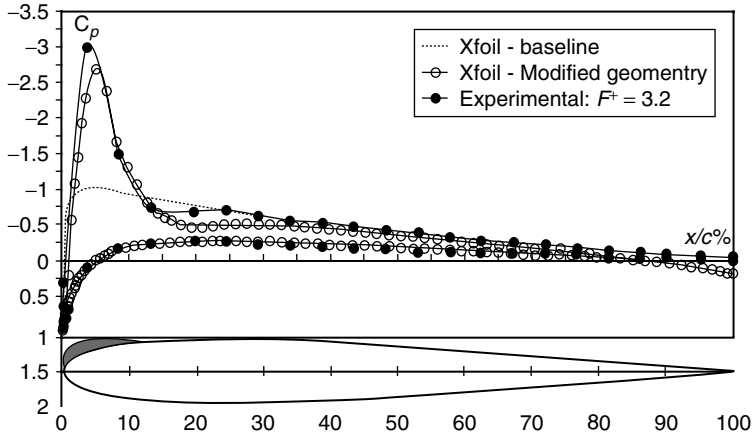

Figure 9. Pressure distribution comparison between synthetic jet virtual shaping and geometrical shaping; $\alpha = 3°$, $Re = 265000$.

From the figure it can be deduced that a synthetic jet based forcing in the vicinity of the leading edge modifies the flow field as effectively as a solid bump does. Both modifications, virtual and real, generate a similar suction peak and also comparable pressure recoveries towards the baseline values after the peak. Compared to a solid modification, the virtual shaping is able to give rise to different pressure distributions around the airfoil giving the possibility to tune appropriately the forcing frequency to the flow conditions in order to generate on demand the most suitable performance of the airfoil.

One reasonable indication of the presence of the virtual aero-shaping, on the base of the pressure distributions, can be obtained by linking the modulus of the minimum value of the pressure coefficient to the non-dimensional forcing frequency F^+ as seen in Fig. 10; curves are shown for incidences 0.5°, 3°, 6° and 9° for the three Reynolds numbers.

As can be observed in Fig.10 the curves exhibit regions of overlapping results for Re = 425000 and for Re = 265000 and also common points at the extreme ends of the portions pertaining to Re = 265000 and Re = 132000, suggesting a not so strong dependence of the formation of the suction region on the Reynolds number. All curves show similar behavior, evidencing increasing values of the suction peak as the frequency increases for all the incidences tested. The effects of the incidence is to shift the curves towards higher values of suction. The significant drop in the value of the suction peak seen for $\alpha = 6°$, Re = 132000 and for a non-dimensional forcing frequency equal to F^+ = 6.4 is due to the strong interaction that causes the bubble breakdown, which in turn determines a large flow separation as indicated by the pressure distribution of Fig. 6.

In general, the virtual shaping is also able to directly influence the drag by introducing high suction near the leading edge. This, in fact, provides a reduction of the pressure drag due to the alleviating component given by the local force acting on the leading upper surface region in the upstream direction.

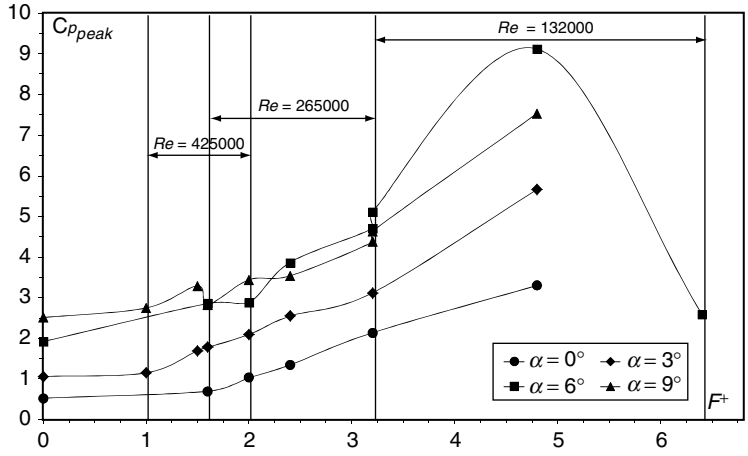

Figure 10. Suction peak values versus F^+ for different Reynolds number and incidences.

3.3. Wake Survey

Results related to the wake surveys are shown for the same cases examined in the previous section. The surveys were conducted for each forcing frequency by positioning the rake in five spanwise sections in the central portion of the wing, in order to measure total pressure distributions, which were then averaged.

In figure 11 the non-dimensional velocity profiles V_w/V_∞ are shown for $\alpha = 3°$ and Re = 265000 in different forcing conditions. The value y/t = 0% corresponds to the trailing edge of the airfoil.

Lower momentum deficit characterizes all the forced cases with respect to the natural flow. The lowest drag coefficient Cd = 0.00982 was obtained for a non-dimensional forcing frequency equal to F^+ = 3.2, evidencing a drag reduction of about 6.5%.

A region, characterized by non-dimentional velocities greater than 1 for F^+ = 2.4 and F^+ = 3.2, which contributes to reduce drag is also evident, especially above the wake. The extension and the values of such velocity overshoot regions appear to increase with the forcing frequency.

Similar wake velocities overshoots are found in many numerical and experimental studies conducted on heaving and/or pitching airfoils. Koochesfahani [23] experimentally investigated the vortical patterns in the wake of a NACA 0012 oscillating airfoil at Reynolds number equal to $1.2 \cdot 10^4$. According

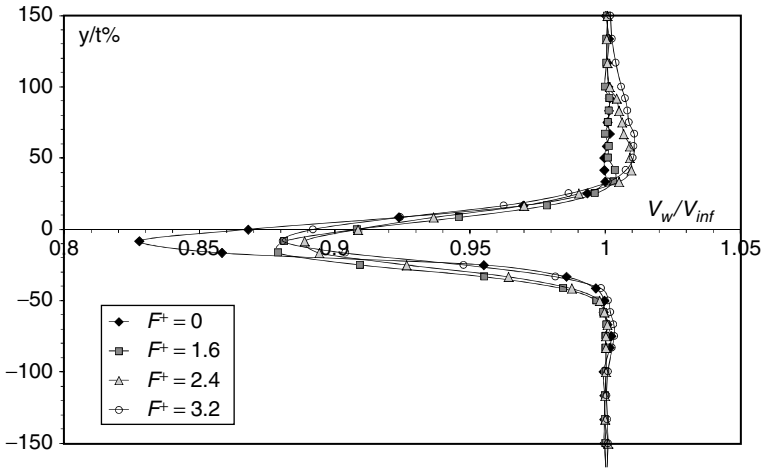

Figure 11. Non-dimensional wake velocity distributions for $\alpha = 3°$, $Re = 265000$ for different forcing conditions.

to the amplitude and the frequency of oscillation, jet-like flow in the wake, which led to drag reduction or thrust generation, was observed. Tuncer and Platzer [18] numerically showed thrust generation by means of a flapping NACA 0012 airfoil at $Re = 3 \cdot 10^6$. Young and Lai [24] numerically studied the plunging effect on the wake of a NACA 0012 airfoil using a compressible 2D Navier Stokes solver at $Re = 2 \cdot 10^4$. In the previous papers the authors observed a wake structure characterized by a particular configuration of vortices that generated jet-like flow in the wake for specific oscillation frequencies. Namely, zero drag or thrust was originated on the airfoil for oscillation frequencies above a threshold level. In the present experiment the velocity overshoot is probably due to the periodic excitation of the synthetic jet which makes the recirculation bubble oscillate around its mean position and size, as revealed by the smoke flow visualizations.

In fact, the instantaneous virtual variation of the airfoil shape on the upper surface near the leading edge generates effects on the wake structure similar to those of oscillating or plunging airfoils [17, 25]. A possible conjecture to explain the drag alleviation our case could be formulated as follows. Spanwise vortices are originated from the direct interaction of the unsteady bubble with the external flow and they are then shed downstream giving rise to the jet-like flow responsible for the velocity overshoot. The unsteadiness of the bubble was evidenced by smoke flow visualization as will be shown later in the paper.

The presence of velocity overshoots in the wake was also observed in the case of synthetic jet flow control over bluff bodies. Amitay *et al*. [26] observed substantial changes in the structure of a cylinder wake when forcing was activated, evidencing a large portion of wake characterized by higher velocities compared to the undisturbed flow. Moreover Amitay [26] also shows a smaller velocity deficit as well as a reduction of the turbulent stresses across the entire wake.

In figure 12 non-dimensional wake velocity profiles are shown for $\alpha = 3°$ and $Re = 425000$.

In analogy with the behavior of the pressure distributions, the benefits of forcing decrease for higher Reynolds number, at least for the frequencies tested. The lower momentum deficit in the wake center for medium and high forcing conditions is evident while for low forcing nearly unchanged velocity distributions were observed. Moreover, regions of drag contribution, centered around y/t = 35%, appear for the three forcing frequencies. These wake regions differ the most with respect to the previous results for Reynolds number equal to 265000. For the same incidence $\alpha = 3°$ and higher Reynolds number, the velocity overshoot regions were not found probably due to insufficient forcing strength. The limitations of the actuators unfortunately did not allow for further investigation in this direction.

The wake survey results at the lowest Reynolds number, for incidence equal to 3° and for $F^+ = 4.8$ are shown in Fig. 13.

In this case the overshoot was clearly and more significantly evidenced, together with a considerable reduction of the momentum deficit in the center of the wake. Due to both contributions, the overall drag reduction achieved in this case was equal to 58%. As can be seen in Fig. 11, Fig. 12, and Fig. 13 the presence or not of jet-like flow in the wake greatly depends on the flow conditions (incidence and Reynolds number) and on the forcing strength. The beneficial effects given by the lower momentum

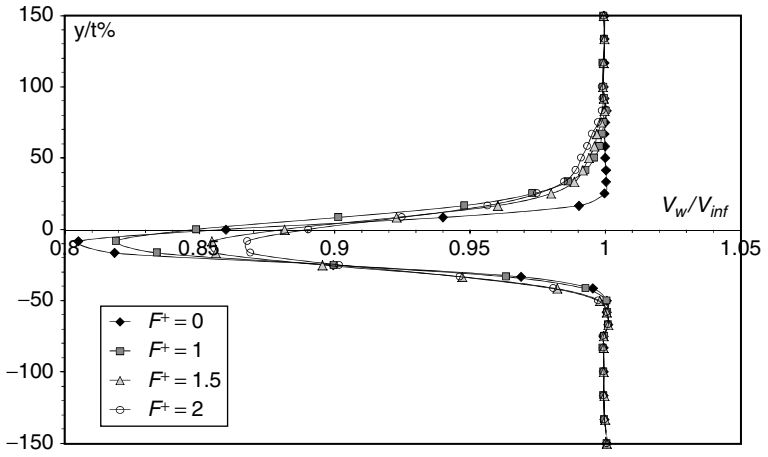

Figure 12. Non-dimensional wake velocity distributions for $\alpha = 3°$, $Re = 425000$ for different forcing conditions.

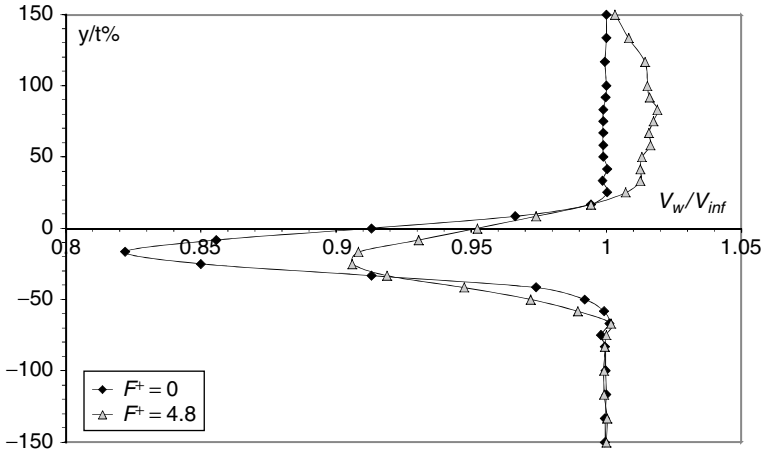

Figure 13. Non-dimensional wake velocity distributions for $\alpha = 3°$, $Re = 132000$. Baseline and forced ($F^+ = 4.8$).

deficit and by the presence of the jet-like flow is related to the availability of sufficient forcing intensity for a given incidence and Reynolds number.

For the same Reynolds number ($Re = 132000$) the effects of the three forcing frequencies in the case of higher incidence, equal to $\alpha = 6°$, were tested.

Figure 14 shows very different velocity distributions in the wake due to different interactions between the external flow and the synthetic jets and directly to the value of the forcing frequency. In the case of lower forcing intensity, namely $F^+ = 3.2$, the momentum deficit decreases in the central part of the wake, giving drag reduction. The increase of the forcing frequency ($F^+ = 4.8$) generates a lower momentum deficit in the middle of the wake up to y/t = 25%, while for y/t > 25% the distribution inverts the trend, giving rise to a drag contribution portion in the wake where the jet-like flow was previously observed. Two different wake characteristics appear, probably originated from two different flows which separate from the upper surface of the airfoil. The interaction between the synthetic jet and the external flow in this last forcing condition is much more complex. It can be conjectured that the interaction probably gives rise to shedding vortices which evolve externally with respect to the attached flow. The attached flow could be responsible for the lower momentum deficit in the middle of the wake while the vortex shedding could be associated with the drag contribution region observed for y/t > 25%.

In the case of the highest forcing ($F^+ = 6.4$) the upper portion of the wake velocity distribution is typical of a large separated flow. In such a forcing condition the synthetic jet breaks up the recirculation bubble causing flow separation on the whole upper surface from the injection slit location.

Finally, as can be observed by comparing the results in Fig.14 with those of the previous figure, giving a higher incidence for the same Reynolds number results in a completely different wake velocity distribution. It is likely that a lower value of the forcing frequency should be used in this case in order to obtain jet-like flow.

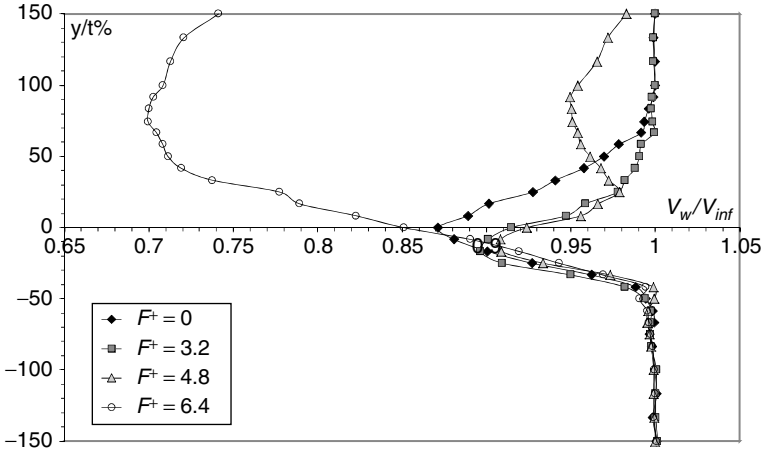

Figure 14. Non-dimensional wake velocity distributions for $\alpha = 6°$, $Re = 132000$ for different forcing conditions.

The observation of the wake structure suggests that different mechanisms responsible for drag reduction can be simultaneously present. Lower momentum deficits in the wake could be associated with the much fuller turbulent boundary layer velocity profile that is caused by the presence of the unsteady bubble. In fact, the bubble oscillations could promote intense mixing at the interface between the external flow and the outer part of the boundary layer, entraining higher level of energy towards the wall flow. As a consequence the boundary layer is fuller and more resistant to separation, which is delayed. In addition to this mechanism, if suitable conditions are present, the occurrence of jet-like flow in the wake can also be present, as previously described.

3.4. Drag Polars

In this section results related to the drag and lift variations under the effect of forcing are presented for the most widely investigated Reynolds number, namely $Re = 265000$. The drag polars for the natural flow and the forced cases are reported in Fig. 15.

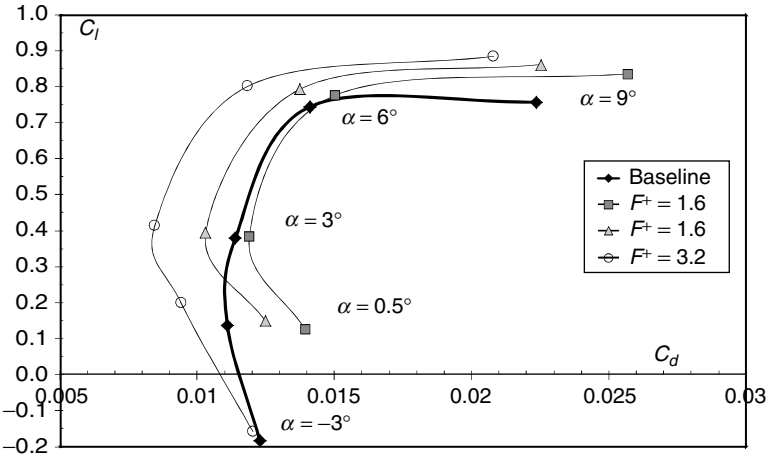

Figure 15. Drag polars for natural and forced flow. $Re = 265000$.

It is evident that for low values of forcing frequency there are positive effects only above a certain value of the incidence. For forcing frequencies as low as $F^+ = 1.6$ the drag results increased for all the incidences tested, while higher lift coefficients are obtained only for angles of attack higher than $\alpha = 6°$. On the other hand, for the maximum value of forcing frequency, the drag polar shows a lift enhancement and a drag reduction in the whole range of angles of attack, although for $\alpha = -3°$ this effect is less marked.

The best results in terms of higher lift to drag ratio are obtained for positive incidences below $\alpha = 6°$. The higher lift enhancement, equal to 46.2%, was achieved for $F^+ = 3.2$ at $\alpha = 0.5°$ even though in this case the variation is very high also for the low value of the lift coefficient at $\alpha = 0.5°$ in natural flow conditions. Lift augmentation is also visible for angles of attack higher than $\alpha = 6°$. The maximum drag reduction, equal to 25.7%, was instead achieved for $F^+ = 3.2$ at $\alpha = 3°$.

The general behavior is the shifting of the drag polars toward regions of lower drag and higher lift as the forcing amplitude is increased.

3.5. Smoke Flow Visualizations

The following pictures show the visualization of the instantaneous flow fields for most of the cases examined in the previous sections. Figure 16 reports four examples of smoke flow visualizations for the incidence $\alpha = 3°$ and $Re = 265000$ in the case of natural and forced flow. The injection location of the synthetic jet in the light sheet plane is evidenced by the red dot.

It was observed that the flow is fully attached both for the natural and the forced cases although in the controlled cases the complete flow field is not shown in order to give a more detailed picture of the injection area, where the interaction takes place.

For all the forced cases the flow begins to deviate when approaching the slit location near the leading edge and determines a modification of the smoke filament evolution showing displacement far from the wall. Subsequently, the flow reattaches generating a recirculation bubble that virtually modifies the local geometry.

A small bubble is still evident in the case of $F^+ = 1.6$ (Fig. 16b) while larger bubbles can be observed for $F^+ = 2.4$ (Fig. 16c) and for $F^+ = 3.2$ (Fig. 16d). In particular for the highest frequency (Fig. 16d) the re-circulating region highlights significant variations also in the wall normal direction.

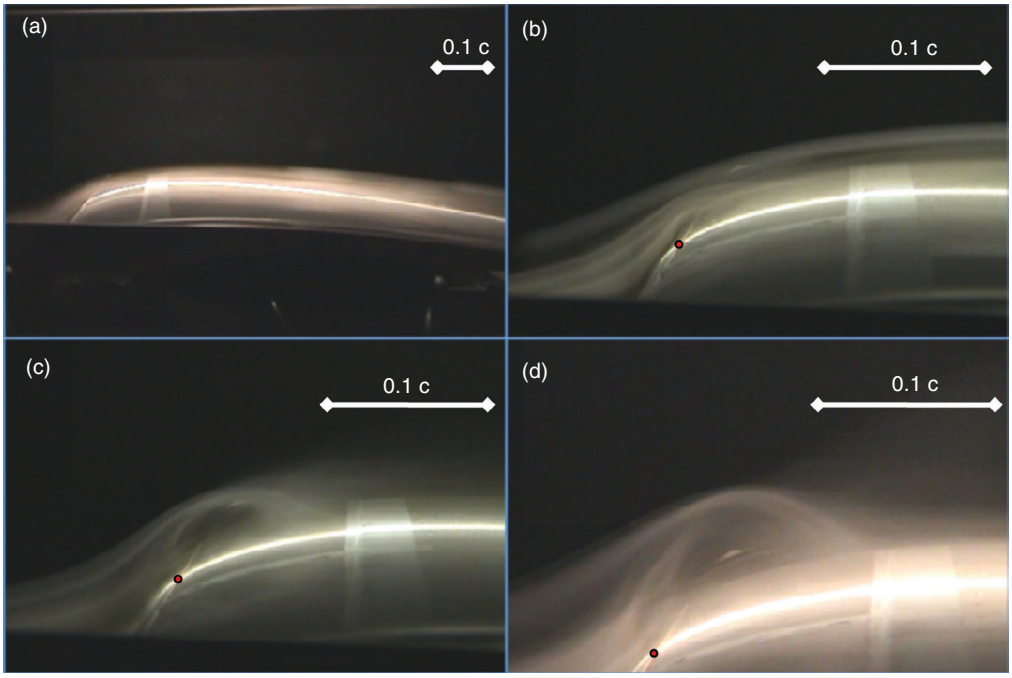

Figure 16. Smoke flow visualizations. $\alpha = 3°$, $Re = 265000$, $(x/c)_{slit} = 1.25\%$. (a) Natural Flow; (b) $F^+ = 1.6$; (c) $F^+ = 2.4$; (d) $F^+ = 3.2$.

The modifications of the flow field evidenced by the flow visualizations are consistent with the pressure distributions of Fig. 3. In fact, the recirculation bubbles increase their size according to the forcing strength similarly to the extension of the suction regions of Fig. 3.

The four cases reported in Fig. 16 are associated to the wake velocity distributions of Fig. 11. All forcing conditions caused reduction of the momentum deficit in the wake. The bubbles produced by non-dimensional frequencies equal to $F^+ = 2.4$ and $F^+ = 3.2$ (Fig. 19c and Fig. 19d) are those related to the interaction responsible for the jet-like flow in the wake.

As shown in Fig. 17, for RE = 425000 the forcing becomes less effective due to the lesser strength of the synthetic jet compared to the momentum of the external flow. As can be observed, the recirculating flow regions are evident in all forced cases but their sizes are much smaller compared to those pertaining to the previous Renolds number. Also in this case the sizes of the bubbles increase with the forcing frequencies. Smaller bubbles are related to less intense suction regions and also to lower momentum deficits in the wake as evidenced from the pressure distributions of figure 4 and from the wake velocity distribution of figure 12.

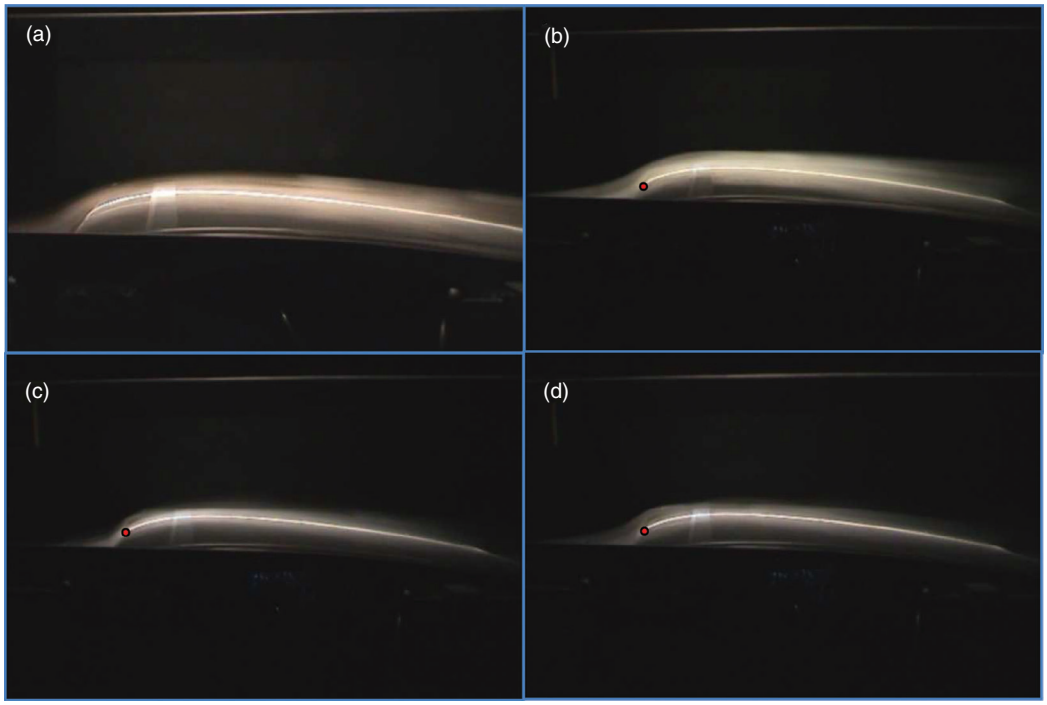

Figure 17. Smoke flow visualizations. $\alpha = 3°$, $Re = 425000$, $(x/c)_{slit} = 1.25\%$. (a) Natural Flow; (b) $F^+ = 1$; (c) $F^+ = 1.5$; (d) $F^+ = 2$.

The strongest interaction between the synthetic jet and the external flow is shown in the flow visualizations reported in Fig. 18 which was obtained for the lowest Reynolds number and for an incidence equal to 3°, varying the forcing frequency.

Figure 18a and figure 18c correspond to the pressure distributions of Fig. 5 and to the wake velocity distributions of Fig. 13. When F^+ is equal to 3.2 (Fig. 18b) and to 4.8 (Fig. 18c) the flow is fully attached and a large bubble is present. In particular, for $F^+ = 4.8$, the recirculation bubble reaches a very large size covering a significant portion of the airfoil surface. As can be observed in Fig. 5, this generates a very intense suction region around the injection slit. Furthermore, as shown in Fig. 13, the bubble has a double effect on the wake, namely a lower momentum deficit and a high level of jet-like flow in the upper part of the wake. Fig. 18d shows that for $F^+ = 6.4$, there is a complete separation of the flow from the slit location. In these conditions, the external flow does not possess enough energy to withstand the forcing action and the bubble breaks up originating a massive flow separation covering the whole surface of the airfoil.

To give a qualitative indication of the magnitude of the bubble unsteadiness, three different photograms, taken for $\alpha = 3°$ and $Re = 265000$ at $F^+ = 3.2$, are reported in figure 19.

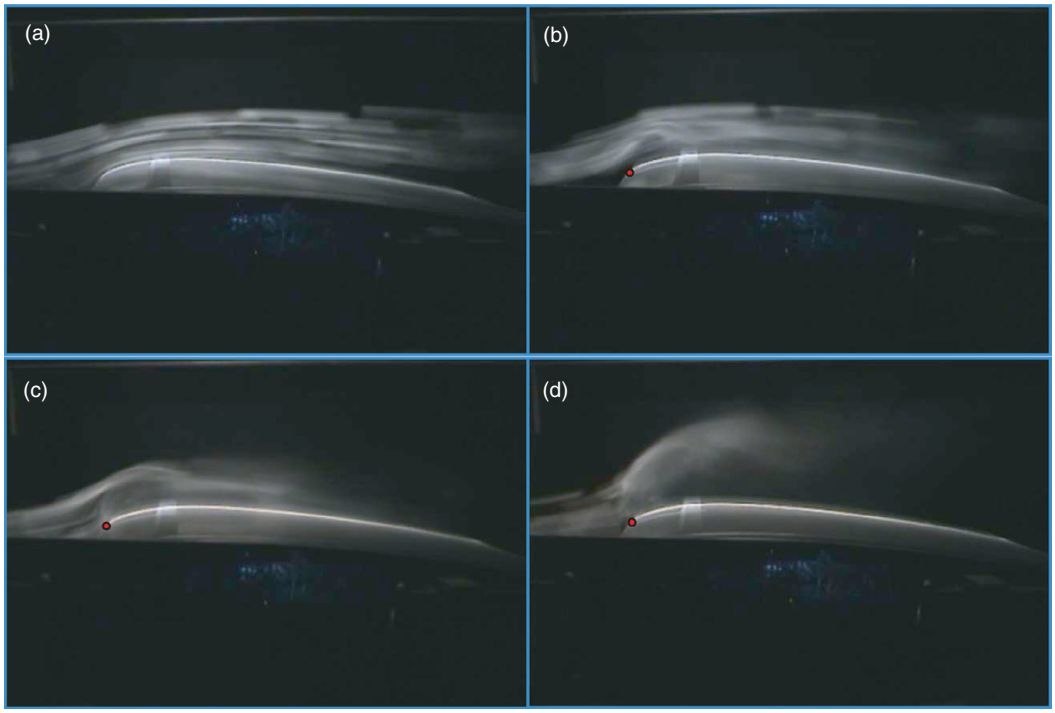

Figure 18. Smoke flow visualizations. $\alpha = 3°$, $Re = 132000$, $(x/c)_{slit} = 1.25\%$. (a) Natural Flow; (b) $F^+ = 3.2$; (c) $F^+ = 4.8$; (d) $F^+ = 6.4$.

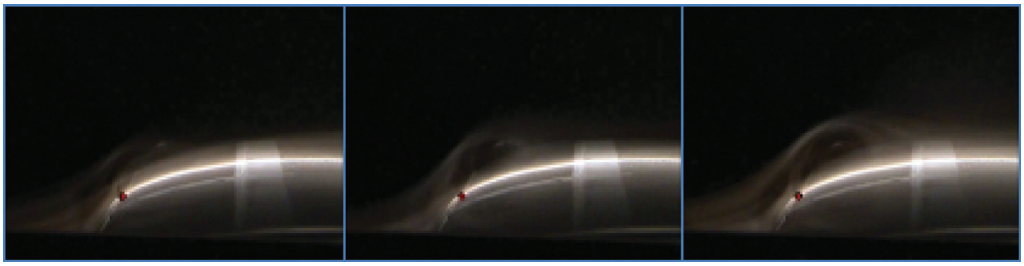

Figure 19. Bubble size unsteadiness. $\alpha = 3°$, $Re = 265000$, $(x/c)_{slit} = 1.25\%$, $F^+ = 3.2$.

The bubble is unsteady, it oscillates and constantly undergoes small variations in shape and size. The observed unsteadiness of the bubble in the present experiment was also highlighted in the results of Honohan *et al*. [11]. The authors observed the formation of quasi steady recirculation regions for Stokes numbers greater than 10. Using the same definition given by the authors, namely $S = \sqrt{\omega h^2/\nu}$ where ω is the angular frequency and ν is the kinematic viscosity, for the present experiment the Stokes number ranges from 4.16 to 5.89.

Flow visualizations confirm that the virtual shaping can be created by the interaction between synthetic jets and the flow around the leading edge which gives rise to a re-circulating flow capable of displacing the streamlines, modifying the pressure distribution around the leading edge and considerably changing the wake structure. The average size and shape of the bubble depend on the forcing frequency, on the incidence and on the Reynolds number. Studies conducted by Glezer and Amitay [2], Mittal and Rampunggoon [16], Cui *et al*. [20] among others, also demonstrated that the formation of recirculation bubbles gives rise to the virtual shaping which takes place when the non-dimensional forcing frequency F^+ is at least in the order of 1.

3.6. Scaling Law

An attempt for the evaluation of a simple scaling law was carried out focusing on the ability of the synthetic jet to create re-circulating bubbles. For this purpose we considered the virtual shaping

responsible for the suction region around the leading edge and for this analysis we used only those results related to the presence of suction regions associated with reduced momentum deficit in the wake. The scaling law links the mean bubble size to the forcing parameters and the flow conditions (Reynolds number and incidence).

Mittal and Rampunggoon [16], in the case of a flat plate with a laminar boundary layer forced with a synthetic jet, observed that the bubble length increased with the jet momentum flux and decreased on increasing the streamwise momentum flux of the boundary layer. The authors proposed a scaling law linking the non-dimensional streamwise bubble size to the ratio between the jet momentum flux and the streamwise momentum flux of the boundary layer at the injection, evidencing a linear growth of the normalized bubble length with the momentum coefficient.

In the following we explore this scaling law for our results defining the same parameters introduced by the Mittal and Rampunggoon [16]. The streamwise length of the bubble L is made dimensionless using the slit width h. The momentum coefficient was defined as suggested by the authors:

$$C_{\mu\theta} = \frac{hV_j^2}{\theta V_\infty^2} \tag{3}$$

In our case only a rough estimation can be made for the bubble length and the momentum thickness of the boundary layer θ. The length L of the bubble is estimated by evaluating the streamwise extensions of the suction regions near the leading edge in the pressure distribution results. Considering the distance of the pressure taps around the slit, the maximum error in the estimation of the bubble length was 10% for the smallest bubble size.

In order to estimate the momentum thickness it is assumed that from the stagnation point up to the slit injection, positioned at $x/c = 0.0125$, the boundary layer was laminar due to the great external flow acceleration. Moreover we also assume that the boundary layer momentum thickness at the slit injection, maintains roughly the same value pertaining to the stagnation point due to the closeness between the two points. Given that, for a laminar boundary layer the momentum thickness in the stagnation point is evaluated considering the Thwaites integral method which leads to the simple relation:

$$\theta = \sqrt{\frac{0.45\nu}{6a}} \tag{4}$$

where a is the gradient of the external velocity at the stagnation point. This last quantity was estimated from the pressure distributions.

The momentum thickness of the boundary layer varies along the airfoil surface in accordance with the incidence and with the Reynolds number. In this analysis the effects of both flow parameters are taken into account in the evaluation of the momentum thickness.

In Fig. 20 the present data are reported in a base ten logarithmic diagram as proposed by Mittal and Rampunggoon [16]. The best fitting line is also showed on the same plot.

As can be observed even though a degree of spreading of the results is evident, a clear trend of linear behavior is highlighted as in the results of Mittal and Rampunggoon [16]. In their case the slope was equal to 1.03 while the present analysis shows a lower slope of about 0.5. The different value of the slope can be attributed to the different body tested and also to the effects of the incidences and the different Reynolds numbers.

It appears that the boundary layer momentum thickness is the most appropriate choice for the definition of the momentum coefficient that leads to the virtual shaping because the physical process governing the formation of the bubble depends on the momentum exchange that takes place during the interaction between the synthetic jet and the incoming boundary layer.

In figure 21, analogously to the previous results, the bubble length L/h is displayed as a function of the non-dimensional forcing frequency F^+ in a logarithmic diagram.

For this data the best fitting is reported on the same figure. Also in this case a linear trend showing a higher value of slope compared to the previous diagram can be seen. The results of Fig. 20 and Fig. 21 define the criteria under which, for the present airfoil, the bubble formation takes place from the

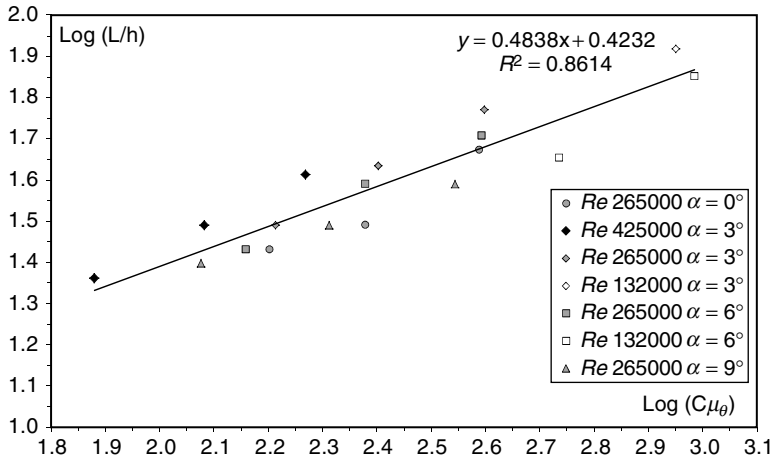

Figure 20. Variation of non-dimensional bubble length versus the momentum coefficient.

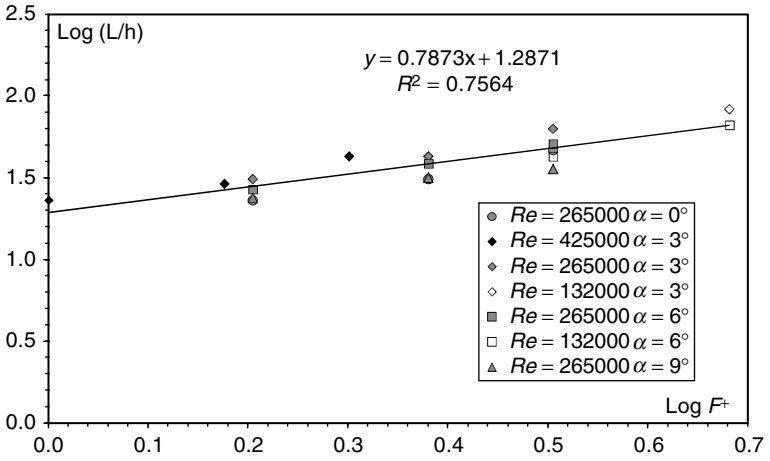

Figure 21. Variation of non-dimensional bubble length versus F^+.

interaction between the synthetic jet and the main stream in accordance with the value of the forcing parameters.

In the following two figures, 22 and 23, the data points reported for the scaling laws have been used to display the effects of the presence of virtual shaping on the drag and lift coefficient variations with respect to the unforced conditions, as a function of the momentum coefficient.

As can be observed even though a spreading of the data is present, especially for the lift variations, a linear trend is evident for both coefficients. Moreover, the presence of virtual shaping does not always improve the aerodynamic performances of the airfoil. In fact, as can be seen for the present experiment, drag reduction and lift enhancement can be achieved only if the values of $C_{\mu\theta}$ are greater than a certain threshold. In effect, negative values of $\mathrm{Log}(C_d/C_{dnf})$ are evidenced for $\mathrm{Log}(C_{\mu\theta}) > 2.35$ while for the lift enhancement the threshold value is around 2.2, not very different from the previous value.

A wider range of investigations involving other classes of airfoils, different actuators and in particular higher Reynolds numbers would be necessary to verify similar scaling laws associated with drag and lift variations. Such results would be a very useful guideline to the design of the actuator and to the employment of synthetic jets. This flow control technique appears very powerful due to the possibility of actuation on demand with the most appropriate forcing strength in accordance with the flow conditions.

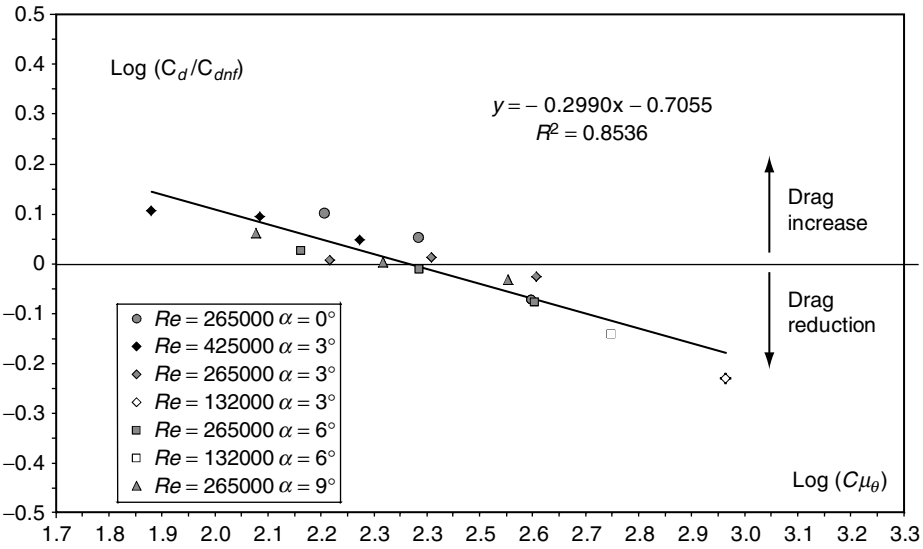

Figure 22. Drag variations in presence of virtual shaping.

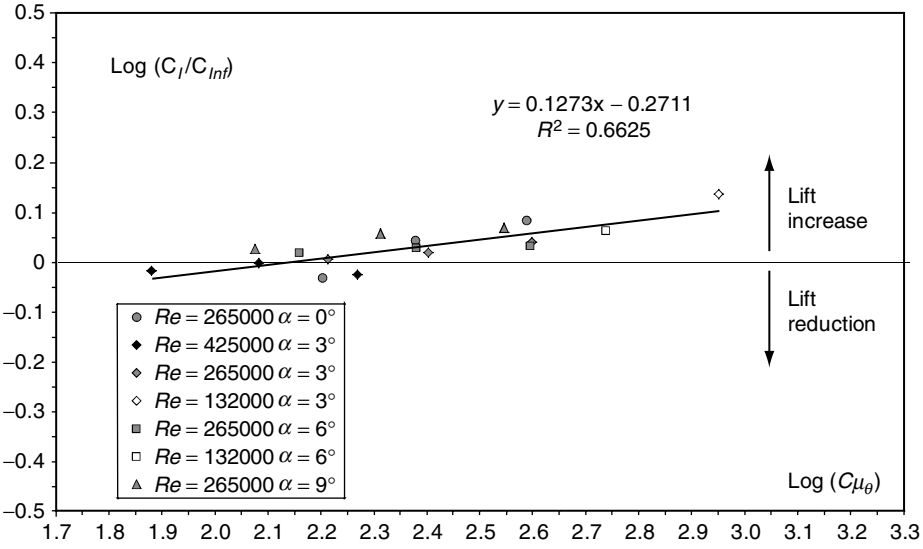

Figure 23. Lift variations in presence of virtual shaping.

4. CONCLUSIONS

An experimental study was carried out to investigate the effects produced by high power synthetic jet forcing on the flow field over a NACA 0015 wing profile. Pressure measurements, wake surveys and flow visualizations were performed for different forcing frequencies and flow conditions.

Flow visualizations showed the formation of a recirculation bubble created by the interaction between the synthetic jet and the external flow. Such structure was capable of displacing the streamlines, generating the virtual shaping phenomenon. The bubble size was much greater when the injection slit was located in the neighborhood of the leading edge, at x/c = 1.25%, while it was dramatically reduced when the injection location was moved downstream. Eventually, when strong forcing was applied, the break-up of the recirculation bubble occurred, causing flow separation with a dramatic increase in drag and only marginal effect on lift. Furthermore, flow visualizations evidenced the unsteadiness of the recirculation bubble.

Pressure distributions around the airfoil were consistent with the presence of a recirculation bubble near the injection location. In fact, high suction regions were observed and attributed to local deflection of the streamlines around the leading edge downstream of the injection slit. It was found that, for $(x/c)_{slit} = 1.25\%$, the minimum value of forcing for which bubble formation was evidenced decreases with the incidence, while the opposite behavior seems to characterize the case for $(x/c)_{slit} = 10\%$.

The wake analysis showed some interesting features, including a lower momentum deficit when forcing was active. This could be a result of a delayed separation on the upper surface promoted by a fuller boundary layer profile caused by the interaction of the external flow with the synthetic jet. Furthermore, under certain flow and forcing conditions, an overshoot of velocity, causing drag reduction, was observed. In fact jet-like flow, similar to those typical of oscillating airfoils, was found in the wake. It can be conjectured that this behavior is due to spanwise vortices, generated by the instantaneous variations in the shape of the bubble, which are shed in the wake.

The virtual shaping effect was characterized by introducing a simple scaling law, relating the non-dimensional bubble size L/h to the momentum coefficient $C_{\mu\theta}$ based on the boundary layer momentum thickness θ at the injection point. A linear trend with a slope of about 0.5 was observed in the log-log plane. The lift and drag variations associated with the presence of virtual shaping also showed linear trends with $C_{\mu\theta}$, highlighting threshold values of the momentum coefficient over which drag reduction and lift enhancement can be achieved. This scaling law should be further investigated for a wider range of forcing conditions and higher Reynolds numbers including other classes of airfoils and different actuators in order to generalize the possible effects of virtual shaping on airfoils.

ACKNOWLEDGEMENTS

The project was financially supported by Regione Piemonte-Bando 2004 (Project E40). Thanks are due to M. Masili and M. Grivet having provided their help during the experimental investigations.

NOMENCLATURE

B = test chamber width [m]
b = wing span [m]
c = wing chord [m]
C_p = pressure coefficient
C_μ = momentum coefficient based on wing chord
C_θ = momentum coefficient based on boundary layer momentum thickness
f = dimensional forcing frequency [Hz]
F^+ = non-dimensional forcing frequency
h = synthetic jet's injection slit width [mm]
L = streamwise bubble dimension [mm]
Re = Reynolds number based on wing chord
S = Stokes number
t = wing thickness [m]
V_∞ = freestream velocity [m/s]
V_j = mean synthetic jet velocity [m/s]
V_w = mean flow velocity in the wake [m/s]
α = angle of attack [deg]
θ = momentum thickness of the boundary layer

REFERENCES

[1] Smith, B. L. and Glezer, A. "The Formation and Evolution of Synthetic Jets", Phys. Fluids , Vol. 10, No.10, 1998, 2281–2297.

[2] Glezer A. and Amitay M. "Synthetic jets", Annual Review of Fluid Mechanics, Vol. 34, 503–529, January 2002.

[3] Cater J.E., Soria J., "The Evolution of Round Zero-Net-Mass-Flux Jets", Journal of Fluid Mechanics, Vol. 472, 167–200, 2002.

[4] Rizzetta, D. P., Visbal, M.R., and Stanek, M.J., (1999), "Numerical Investigation of Synthetic-Jet Flowfields." AIAA Journal, 37.8, 919–927.

[5] Seifert A., Darabi A., and Wygnanski, I., "Delay of Airfoil Stall by Periodic Excitation", Journal of Aircraft, Vol. 33, No. 4, 1996, 691–698.

[6] Trávníček Z., Tesař V., "Annular Synthetic Jet used for impinging flow mass-transfer", International Journal of Heat and Mass Transfer, 46 (2003) 3291–3297.

[7] Glezer A., "Fluidic-Based Virtual Aerosurface Shaping", RTO-MP-AVT-111.

[8] Glezer A., Amitay M., and Honohan, A., "Aspects of Low- and High- Frequency Aerodynamic Flow Control", AIAA Journal, vol. 43, No. 7, 2005, 1501–1511.

[9] Smith D., Amitay M., Kibens V., Parekh D., and Glezer A., "Modification of Lifting body Aerodinamics using Synthetic Jets actuator", AIAA paper 2003–0533, 2003.

[10] Honohan A., "The interaction of Synthetic Jets with Cross Flow and the Modification of Aerodynamic Surface", PhD dissertation, Georgia Institute of Tecnology, Atlante, GA, 2003.

[11] Honohan A., Amitay M., and Glezer, A., "Aerodynamic control using Synthetic Jets", AIAA paper 2000–2401, Fluids 2000 conference, Denver, CO, 2000.

[12] Rehaman A., Kontis K., "Synthetic Jets Control Effectiveness on Stationary and Pitching Airfoils", Journal of Aircraft, Vol. No. 46, November – December 2006.

[13] Gilarranz J.L. and Rediniotis O.K., "Characterization of a Compact, High-Power Synthetic Jet Actuators for Flow Separation Control", AIAA 2001–0737, 2001.

[14] You D. and Moin P., "Large-eddy simulation of flow separation over an airfoil with synthetic jets control", Journal of Fluids and Structures 24 (2008), 1349–1357.

[15] Duvigneau R., Visonneau M., "Simulation and optimization of stall control for an airfoil with a synthetic jet", Aerospace Science and Technology 10 (2006), 279–287.

[16] Mittal R., Rampunggoon P., "On the Virtual Aeroshaping Effect of Synthetic Jets", Phys. Fluids, Vol. 14, No. 4, April 2002, 1533–1536.

[17] Holman R., Utturkar Y., Mittal R., Smith B.L., Cattafesta L., "Formation Criterion for Synthetic Jets", AIAA Journal, Vol. 43, No.10, October 2005.

[18] Tuncer I. H., Platzer M. F., "Thrust Generation due to Airfoil Flapping", AIAA Journal, Vol. 34, No. 2, February 1996.

[19] Ciuryla M., Liu Y., Farnsworth J., Kwan C., Amitay M., "Flight Control Using Synthetic Jets on a Cessna 182 Model", Journal of Aircraft, Vol. 44, No. 2, March–April 2007.

[20] Cui J., Agarwal R. K., Cary A.W., "Numerical Simulation of the Interaction of a Synthetic Jet with a Turbolent Boundary Layer", AIAA 2003–3458.

[21] Akçayöz E., Tuncer I. H., "Numerical Investigation of Flow Control over an Airfoil using Synthetic jets and its Optimization", AIAC-2009–043.

[22] Gordon M., Soria J., "PIV Measurements of a Zero-Net-Mass-Flux Jet in Cross Flow", Experiments in Fluids 33 (2002) 863–872.

[23] Koochesfahani M. M., "Vortical Patterns in the Wake of an Oscillating Airfoil", AIAA Journal, Vol. 27, No. 9, February 1989.

[24] Young J., and Lai. J. C. S., "Oscillation Frequency and Amplitude Effects on the Wake of a Plunging Airfoil", AIAA Journal, Vol. 42, No.10, October 2004.

[25] Jones K.D., Dohring C.M. and Platzer M.F., "Wake Structures Behind plunging Airfoils: A Comparison of Numerical and Experimental Results" , AIAA paper 96–0078.

[26] Amitay M., Smith B. L., Glezer A., "Aerodynamic Flow Control Using Synthetic Jet Technology", AIAA Paper 98–0208, Jan. 1998.